Acta Acustica 2026, **10**, 62
© The Author(s), Published by EDP Sciences, 2026
https://doi.org/10.1051/aacus/2026059

Available online at:
https://acta-acustica.edpsciences.org

Topical Issue - Proceedings of AFPAC 2026

SCIENTIFIC ARTICLE OPEN ACCESS

Numerical characterisation of elastic wave propagation in fibre-textured polycrystals: Example of complex-valued stiffness evolution with microstructural parameters

Nicolas Leymarie*, Vincent Dorval, Jordan Barras, Alexandre Imperiale, and Edouard Demaldent

Université Paris-Saclay, CEA, List, F-91120 Palaiseau, France

Received 30 March 2026, Accepted 12 June 2026

Abstract – The study of elastic wave propagation in polycrystalline media and the modelling of associated scattering phenomena has gained renewed interest over the past decade, driven by advances in computational capabilities enabling Finite Element (FE) simulations on statistically representative microstructures. These approaches have made it possible to analyse complex polycrystalline materials with varying anisotropy and to compare numerical results with existing analytical models. Most studies have focused on the estimation of wavenumber evolution across frequency regimes for untextured media and coherent longitudinal waves. More recently, extending these approaches to shear waves has enabled a complete numerical characterisation of an effective isotropic medium. At the macroscopic scale, such effective properties can be directly used in numerical methods, including high-order FE or high-frequency ray-based approaches, to simulate ultrasonic testing (UT) of components whose dimensions largely exceed the characteristic grain size. However, for textured polycrystalline media, most investigations remain restricted to wave propagation along symmetry axes. The modelling and extraction of modal solutions become significantly more complex when multiple coherent wave modes coexist. In the case of fibre-textured media described by a Gaussian Orientation Distribution Function (ODF), we have recently developed an original numerical framework to address these challenges. By analysing wave propagation in different directions, an effective transversely isotropic medium is identified, whose complex-valued properties reproduce the estimated wavenumbers. This work investigates the evolution of the associated stiffness tensor components with respect to the ODF parameters and discusses potential applications for the characterisation of austenitic welds and claddings in UT simulations and imaging.

Keywords. Wave scattering, Fibre-textured polycrystal, Effective material characterisation, Complex-valued stiffnesses

1 Introduction

Austenitic stainless steels widely used in industrial components such as claddings and welded assemblies often exhibit pronounced microstructural anisotropy resulting from solidification and thermomechanical processing. These materials typically display elongated grains associated with a strong fibre texture aligned with the elongation direction. Such microstructural features are well known to significantly affect ultrasonic testing (UT) methods. At the ultrasonic wavelengths typically employed in UT, the scattering regime governing wave propagation often falls within the Rayleigh regime or transitions into the early stochastic regime. The anisotropic properties of single grains and their differences in orientations significantly perturb the propagation of coherent wavefronts, particularly when the microstructure exhibits an anisotropic fibre texture. As a consequence, ultrasonic beams may exhibit strong deviations, beam splitting phenomena related to spatial variations of elastic anisotropy, as well as anisotropic attenuation caused by grain scattering and the generation of significant structural noise. These effects represent major challenges for reliable ultrasonic inspection and modelling, particularly in welded austenitic components used in safety-critical components.

In this context, full-scale modelling of UT propagation based on an explicit grain-scale description of the microstructure is neither practical nor computationally tractable when considering components of industrial dimensions. Such microscale approaches, while physically accurate, lead to prohibitive computational costs and are therefore not suitable for intensive simulation plans.

*Corresponding author: nicolas.leymarie.@cea.fr

As a result, a more computationally efficient strategy is employed. It consists in representing the polycrystalline material as an equivalent effective medium, which may be isotropic or anisotropic depending on the underlying microstructural texture. UT propagation in this medium can be simulated using finite element methods, accelerated by eliminating the need for a grain-scale mesh, or alternatively approximated efficiently with fast ray-based analytical techniques. To account for energy losses induced by wave scattering at the grain scale, attenuation of the coherent wavefront is considered through the definition of an effective complex wavenumber, encompassing both phase velocity and attenuation. Analytical scattering theories have been developed to estimate these effective properties in polycrystalline materials [1, 2]. However, the validity of such analytical models is generally confined to materials exhibiting limited elastic contrast between grains. The role of crystallographic anisotropy, notably through its impact on the elastic scattering coefficient, has been thoroughly investigated in a recent study [3]. These models have been applied to microstructure with elongation [4–6] or texture [7–9], requiring dedicated theoretical developments tailored to each type of microstructure description. The intricacy of applying these models to potentially complex microstructures, along with the inherent limitations arising from their approximations, motivates the use of numerical approaches that can explicitly capture wave-microstructure interactions for any given material. Finite element (FE) simulations have therefore increasingly been employed to investigate ultrasonic scattering in polycrystalline media. Numerical studies, notably performed using the POGO simulation framework, demonstrated the capability of such approaches to capture grain scattering in three-dimensional simulations and to estimate coherent wave properties in equiaxed, non-textured polycrystalline microstructures representative of isotropic media [10, 11]. Following on from this, numerical investigations have been extended to textured materials with elongated grains, highlighting the important influence of microstructural anisotropy on wave propagation behaviour [5, 12]. Building upon these developments, we first introduced a dedicated numerical framework allowing the estimation of coherent wavenumbers for both longitudinal and shear waves in equiaxed polycrystalline aggregates [13]. This methodology was subsequently extended to anisotropic microstructures combining elongated grains and crystallographic texture, enabling the numerical characterisation of quasi-longitudinal and quasi-shear wave modes in textured polycrystals [14].

The newly developed numerical tool produces direction-dependent velocities and attenuations, which still require translation into an equivalent constitutive law for an anisotropic, damping elastic medium. Within this framework, a key issue is whether such an effective anisotropic medium can be described using conventional elastic constants, and how the associated effective parameters evolve with the underlying microstructural texture. Addressing this question is essential for improving the realism of ultrasonic beam propagation models and, ultimately, for enhancing the predictive capabilities of UT simulation tools applied to complex industrial components. The present contribution aims to address this question by proposing and analysing an effective anisotropic description of coherent wave propagation in virtual textured polycrystalline media.

2 Numerical characterisation effective material properties

2.1 Wavenumber estimations for grain-elongated textured polycristals

To study ultrasonic wave scattering in textured polycrystalline materials, we employ the same numerical framework based on FE simulations of Representative Volume Elements (RVEs). The methodology proposed for the numerical characterisation of coherent wavenumbers in textured polycrystalline microstructures relies on a combination of FE simulations and advanced signal processing techniques. Below we summarise the key principles and methodological steps relevant to the proposed study. For further details, all these steps are fully described in theses articles [13–15].

The approach begins with the generation of spatially periodic RVEs which are designed to capture statistically the essential microstructural features of the material under investigation. These RVEs are constructed using random Voronoi tessellations, where each Voronoi cell corresponds to an individual grain within the polycrystalline material. To account for grain elongation, a common feature in materials subjected to mechanical processing such as rolling or welding, a spatial transformation is applied to the Voronoi tessellation. This transformation elongates the grains along a specified direction, typically aligned with the fibre texture axis observed in industrial components. The resulting RVEs are defined as rectangular parallelepipeds and projected onto a regular grid mesh with a uniform step size. A sufficient number of RVEs, typically on the order of fifty or more, is generated to guarantee statistical convergence of the results. This accounts for natural variations in grain shape and crystallographic orientation distributions, which are essential for accurately representing the statistical properties of the polycrystalline material. The use of multiple RVEs allows for averaging out random fluctuations and ensures robust estimates of coherent wave properties.

The simulation of plane wave (PW) propagation through the textured microstructure requires specific boundary conditions to be applied to the RVE. A uniform stress pulse is applied to the top surface of the RVE, normal to the z-axis, simulating the excitation of a plane wave. This loading is designed to simultaneously excite all anisotropic modes, including quasi-longitudinal, quasi-shear vertical, and quasi-shear horizontal waves, which is essential for characterizing the full wave behaviour in anisotropic media. Periodic boundary conditions are imposed on the lateral faces of the RVE, ensuring that both the elastic properties of the microstructure and the displacement field are periodic. This periodicity is critical for simulating plane-wave propagation in an effectively infinite medium. Other commonly used boundary conditions, such as symmetric ones, fail to capture the behaviour of quasi-shear waves and of quasi-longitudinal whose polarizations may not align with the propagation direction. A free boundary condition is set at the bottom surface of the RVE, although it does not influence the result.

The final step of the methodology involves analyzing the coherent PW field extracted from the FE simulations to determine the effective wavenumbers. The displacement fields computed from the simulations are averaged over the lateral dimensions of the RVE to isolate the coherent PW field. This averaging process reduces the influence of incoherent scattering and highlights the modal contributions of the coherent wavefronts. The averaged displacement fields are then projected onto the modal polarizations derived from Hill's approximation of the polycrystalline material. This modal projection step is crucial for separating the contributions of the quasi-longitudinal, quasi-shear vertical, and quasi-shear horizontal modes, which are inherently coupled in anisotropic media.

The phase evolution of the coherent PW field with depth, along the z-axis, is analyzed to determine the phase velocity of each mode. This is achieved by fitting the phase shift as a function of depth and frequency, providing a direct measure of the real part of the effective wavenumber. Similarly, the amplitude decay of the coherent wave with depth is analyzed to quantify attenuation, which is related to the imaginary part of the effective wavenumber (see [15] for more details). This analysis accounts for scattering-induced energy losses due to grain-scale heterogeneities and provides a measure of how strongly the wave is attenuated as it propagates through the microstructure.

The wave always propagates from the top surface to the bottom, and the computation is repeated for a range of microstructure orientations to characterize the behaviour of plane waves as a function of their propagation angle relative to the texture and elongation directions.

2.2 Application case parameters

The study considers a set of RVEs designed to capture the microstructural features of austenitic steel, which is widely used in industrial components such as welds and claddings. This section presents the practical application focusing on the influence of fibre texture intensities on the coherent wave properties. The single-crystal properties of austenite [16] serve as the basis for generating the polycrystalline microstructures (see Tab. 1).

The set of RVEs considered is defined as follow to ensure statistical relevance and anisotropy identification:

Table 1. Single-crystal elastic properties considered for austenitic stainless steel [16].

ρ (g cm^{-3})	C_{11} (GPa)	C_{12} (GPa)	C_{44} (GPa)
7.958	207	133	117

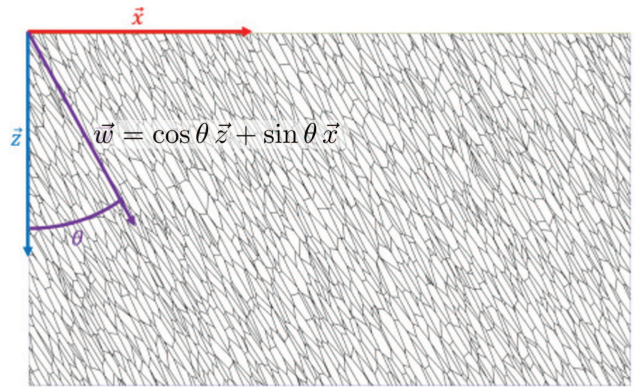

Figure 1. Example of a cross-section in the xz-plane of a REV with grains oriented at 30°.

- A large number of RVEs is generated to guarantee statistical convergence, with $N_V = 50$ distinct realisations for each texture configuration.
- The RVE dimensions are 24 mm × 8 mm × 14 mm, discretised using a voxel step of 60 μm, a discretisation criterion discussed in [14] as the best compromise between computational accuracy and performance, resulting in over 12 million voxels per RVE.
- A fixed elongation factor of $E = 5$ is applied along the elongation axis, denoted as the w-axis (see Fig. 1), yielding dimension statistics given in Figure 2. The angle θ between the wavefront direction and the elongation axis is varied from 0° to 90° in increments of 5°, yielding $N_\theta = 19$ distinct angles.

To investigate the influence of fibre texture intensity, the crystallographic orientations of the grains are modelled using a Gaussian distribution centred around the grain elongation w-axis. This distribution is applied to the second Euler–Bunge angle, Φ, with the orientation distribution function F given by:

$$F_{\mathrm{ODF}}(\phi_1, \Phi, \phi_2) = \frac{\exp\left(-\Phi^2/2\sigma_\Phi^2\right)}{\sin\Phi\,\sqrt{2\pi}\sigma_\Phi}$$

where σ_Φ represents the standard deviation of the Gaussian distribution and is varied to represent different fibre texture intensities. The values considered for σ_Φ are $\{0°, 5°, 10°, 15°, 20°, 25°, 30°\}$, resulting in $N_{\sigma_\Phi} = 7$ distinct texture configurations, the anisotropy decreasing with increasing σ_Φ.

Each simulation uses a Ricker signal with a central frequency of 2.5 MHz representative of typical UT frequencies. The propagation simulation time is set to 3 μs, allowing the analysis of wave propagation conducted over depths ranging from $z = 0$ to 9 mm for quasi-longitudinal

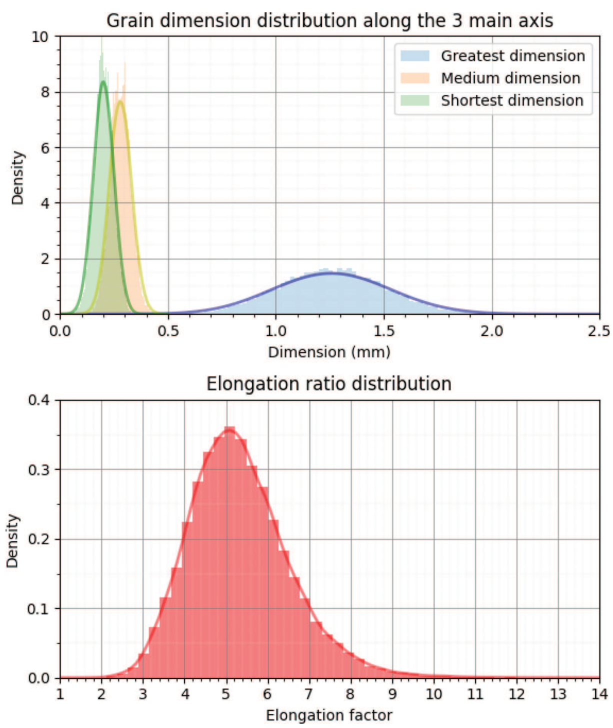

Figure 2. Grain dimension distributions and elongation factor distribution for a given RVE oriented at 30° and containing 400 grains (KDE interpolation in plain lines).

wavefronts and from 0 to 4.5 mm for quasi-shear wavefronts. These modal depths are chosen to ensure that the coherent wavefronts are fully captured within the analysis window.

The computational demands of this study are significant. All simulations were performed on a cluster of six workstations, each equipped with an Intel® Xeon® w5-2455X processor (3.19 GHz, 128 GB RAM). This leads to a total of $N_V \times N_\theta \times N_{\sigma_\Phi} = 6650$ RVEs used in our FE simulations, with each simulation requiring approximately 20 to 30 min (including microstructure generation and FE computation). This results in a total cumulative computation time of around 100 days. However, the simulations are highly scalable and easily distributed across computing clusters, enabling efficient parallelisation and reducing the overall time. Once this calculation is complete, we obtain an estimate of a set of complex wavenumbers characterizing the coherent wavefronts of the quasi-logitudinal (qL), quasi-shear vertical (qSV), and quasi-shear horizontal (qSH) waves for each N_θ direction and for each of the different N_{σ_Φ} textures.

2.3 Material properties identification

Given the slownesses for the three modes and for different directions of the wavefront in the reference frame of the textured polycrystal, we estimate the anisotropic viscoelastic properties that best reproduce the behaviour of coherent waves. The material is modelled as transversely isotropic, with symmetry along the local elongation axis (denoted as the w-axis or axis 3). The effective medium is characterized by five independent complex-valued stiffness parameters denoted: $C_{11}+\mathrm{i}\,\eta_{11}$, $C_{33}+\mathrm{i}\,\eta_{33}$, $C_{13}+\mathrm{i}\,\eta_{13}$, $C_{44}+\mathrm{i}\,\eta_{44}$, $C_{66}+\mathrm{i}\,\eta_{66}$.

The approach relies on classical PW characterisation methods using the Christoffel equation [17] to deduce the values of the three modal slownesses as a function of the five independent complex stiffnesses. The stiffness values are identified using a minimization procedure [18, 19].

The cost function, denoted $F(C_{ij})$, quantifies the difference between the theoretical complex-valued slownesses, $s_m(C_{ij}, \theta_k)$, and the numerical results, $s_m^{\mathrm{FE}}(\theta_k)$, for various propagation directions θ_k and the three identified modes m, and is defined as:

$$F\left(C_{ij}+\mathrm{i}\,\eta_{ij}\right)=\sum_{\theta_k,m}\frac{|s_m\left(C_{ij}+\mathrm{i}\,\eta_{ij},\theta_k\right)-s_m^{\mathrm{FE}}(\theta_k)|^2}{|s_m^{\mathrm{FE}}(\theta_k)|^2}.$$

In practice, the procedure for identifying the stiffness components is summarised in the following steps:

- Global minimisation (Bounded LBFGS) is performed to determine effective real-valued elastic constants with real-valued slownesses. The objective is to match as close as possible the wave velocity, as it is crucial for UT inspection methods. The solutions space is defined in the vicinity of the Hill's approximation.
- Determination of some viscosity coefficients based on the imaginary part of the slownesses along the symmetry axes:

$$\eta_{11}=\rho\,\mathrm{Im}\left(\left[s_{qL}^{\mathrm{FE}}(90°)\right]^{-2}\right),$$
$$\eta_{33}=\rho\,\mathrm{Im}\big(\left[s_{qL}^{\mathrm{FE}}(0°))\right]^{-2}\big).$$

  The objective here is to fit the attenuation of qL waves along the symmetry axes, as qL waves are primarily used in UT inspection methods.
- Partial optimization of the viscosity coefficients η_{13}, η_{44} and η_{66} using Bounded LBFGS.

Several variations of this procedure have been evaluated, yielding equivalent results as long as the optimization is first performed on the real parts only and the fitting of qL waves attenuation is prioritized.

3 Results

3.1 Estimation of velocities and attenuations

The properties estimated using the FE tool for coherent waves are presented for various texture intensities in Figure 3. As expected, the anisotropy of the modes with respect to the propagation direction decreases with increasing σ_Φ. This trend is evident not only in the phase velocities but also in the attenuation, particularly for the qL mode.

As anticipated, the attenuation of coherent waves along the fibre axis also increases with increasing σ_Φ, regardless of the mode considered. Finally, as highlighted

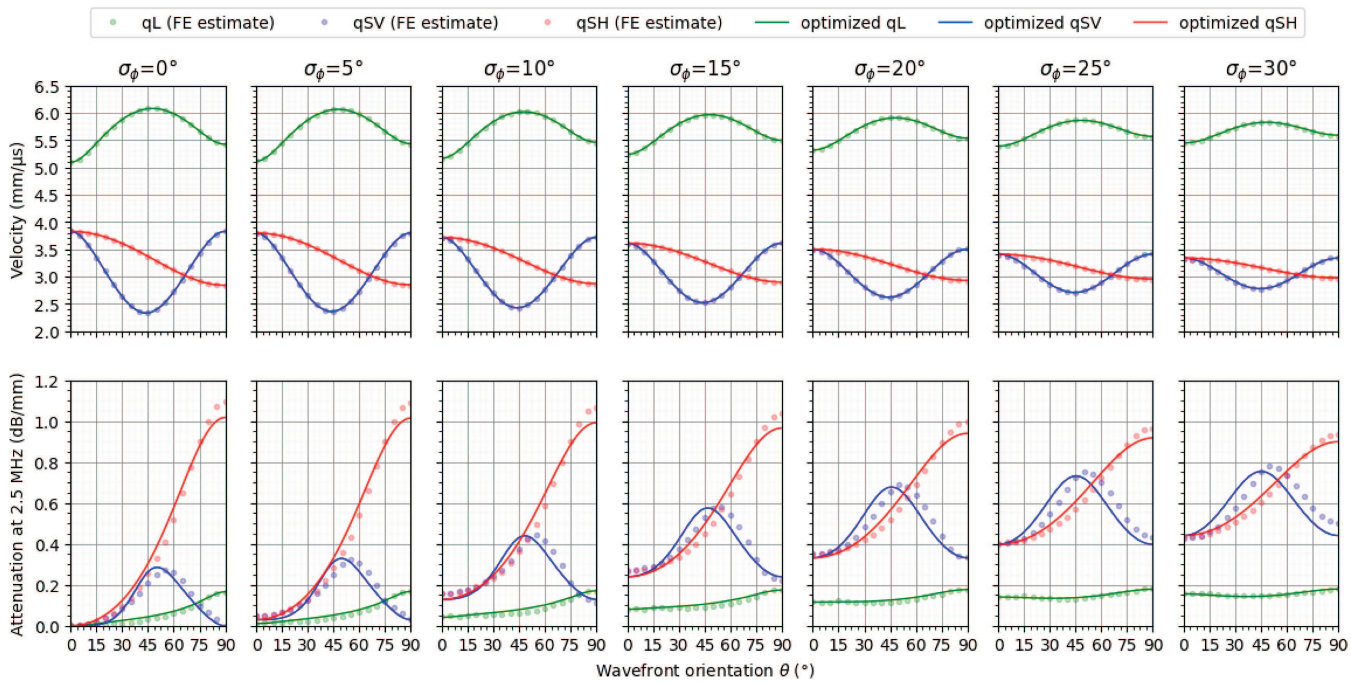

Figure 3. Phase velocities and attenuations of the qL, qSV, and qSH modes for wave propagation directions of 0° and 90°, and for different texture intensities σ_Φ: discrete points correspond to measurements obtained using the FE numerical tool, while solid lines represent the values predicted using the optimised stiffness components.

in [14], for qSV waves, no perfect symmetry is observed between the behaviour of coherent waves propagating at 0° and 90°. We attribute this to the elongation of the grains, which raises questions regarding the compatibility of this dataset with an effective medium described by conventional elastic constants under the assumption of transverse isotropy.

3.2 Characterisation of effective materials for various textures

All the optimised stiffness components characterising the effective material for the various fibre texture intensities are reported in Table 2. The inversion procedure, applied to the seven texture cases considered, is computationally efficient and was completed in approximately ten seconds, without any numerical or convergence issues.

To assess the quality of the characterisation process, the theoretical phase velocities and attenuation values obtained from the optimised stiffness components were compared with the reference data derived from FE calculations shown in Figure 3. This comparison provides a first level of validation of the identified effective material properties through a direct confrontation between model predictions and numerical data. In addition, Table 3 summarises the relative errors in phase velocity and the deviations in attenuation between the effective medium predictions and the FE results.

Overall, excellent agreement is observed for phase velocity predictions across all propagation modes (relative errors below 0.48%), indicating that the effective stiffness tensor successfully captures the dominant elastic behaviour of the medium, including its anisotropic characteristics.

In contrast, the agreement is more nuanced for attenuation. While the effective medium approach yields very satisfactory results for qL waves, with discrepancies remaining below 0.02 dB/mm, larger deviations are observed for shear modes. In these cases, the errors can reach values on the order of 0.08 dB/mm, reflecting a reduced accuracy of the model in capturing dissipative mechanisms associated with transverse wave propagation. These discrepancies are primarily attributed to the assumption of an effectively transversely isotropic medium, which does not fully reproduce the complexity of the numerically estimated response.

4 Discussion

Using the proposed workflow, we have demonstrated the ability to establish a consistent link between the properties of textured polycrystalline microstructures and those of an effective anisotropic medium representative of coherent wavefront propagation. The results were obtained for texture intensities and grain sizes comparable to those typically observed in welded materials, supporting the relevance of the approach for practical applications.

Several important points emerge from this study. First, an excellent agreement is achieved in the identification of phase velocities and their anisotropy, indicating

Table 2. Estimation of the complex-valued stiffness components with respect to the texture intensity σ_Φ at 2.5 MHz where axis 3 denotes the fibre texture axis of the effective medium.

Texture	Stiffness values in GPa				
σ_ϕ	$C_{11} + \mathrm{i}\,\eta_{11}$	$C_{33} + \mathrm{i}\,\eta_{33}$	$C_{13} + \mathrm{i}\,\eta_{13}$	$C_{44} + \mathrm{i}\,\eta_{44}$	$C_{66} + \mathrm{i}\,\eta_{66}$
0°	$234 + \mathrm{i}\,3.08$	$206 + \mathrm{i}\,0.01$	$133 + \mathrm{i}\,0.68$	$116 + \mathrm{i}\,0.00$	$64 + \mathrm{i}\,2.72$
5°	$234 + \mathrm{i}\,3.13$	$208 + \mathrm{i}\,0.17$	$132 + \mathrm{i}\,0.62$	$114 + \mathrm{i}\,0.19$	$64 + \mathrm{i}\,2.73$
10°	$237 + \mathrm{i}\,3.24$	$212 + \mathrm{i}\,0.67$	$130 + \mathrm{i}\,0.45$	$110 + \mathrm{i}\,0.77$	$65 + \mathrm{i}\,2.74$
15°	$240 + \mathrm{i}\,3.38$	$218 + \mathrm{i}\,1.36$	$128 + \mathrm{i}\,0.18$	$103 + \mathrm{i}\,1.32$	$66 + \mathrm{i}\,2.75$
20°	$243 + \mathrm{i}\,3.50$	$226 + \mathrm{i}\,2.03$	$125 - \mathrm{i}\,0.11$	$97 + \mathrm{i}\,1.66$	$68 + \mathrm{i}\,2.76$
25°	$246 + \mathrm{i}\,3.60$	$231 + \mathrm{i}\,2.57$	$122 - \mathrm{i}\,0.32$	$92 + \mathrm{i}\,1.84$	$69 + \mathrm{i}\,2.76$
30°	$248 + \mathrm{i}\,3.66$	$236 + \mathrm{i}\,2.94$	$119 - \mathrm{i}\,0.47$	$88 + \mathrm{i}\,1.92$	$70 + \mathrm{i}\,2.76$

Table 3. Relative velocity errors and attenuation deviations for different texture intensities and for each mode.

Texture	Velocity deviations (mm/μs)						Attenuation deviationss (dB/mm)					
σ_ϕ	qL		qSV		qSH		qL		qSV		qSH	
	Mean	Max	Mean	Max	Mean	Max	Mean	Max	Mean	Max	Mean	Max
0°	1.6	3.3	1.9	4.1	3.2	6.7	0.009	0.015	0.021	0.055	0.034	0.078
5°	2.1	4.8	1.9	3.6	3.6	7.1	0.008	0.015	0.027	0.062	0.034	0.075
10°	3.1	8.3	3.1	7.9	4.3	7.7	0.009	0.018	0.031	0.070	0.036	0.075
15°	4.2	11.1	5.8	13.6	5.0	8.3	0.008	0.018	0.034	0.070	0.033	0.068
20°	4.9	12.5	8.3	16.2	5.1	9.9	0.006	0.013	0.036	0.074	0.027	0.055
25°	5.2	12.2	9.8	16.6	5.0	10.5	0.003	0.007	0.045	0.079	0.022	0.044
30°	5.0	11.0	10.3	16.0	4.7	10.3	0.002	0.006	0.054	0.082	0.021	0.035

that the effective medium accurately captures the dominant elastic behaviour of the material. A good agreement is obtained for the attenuation of qL waves. The effective medium approach proves capable of reproducing the anisotropic variations associated with scattering phenomena affecting longitudinal waves. However, a more significant lack of accuracy is observed for the attenuation of shear waves (qSV and qSH). This limitation highlights the increased complexity of modelling dissipative mechanisms associated with transverse wave propagation.

The identified stiffness tensor components can be directly incorporated into macroscopic models of welded structures [20, 21]. At this scale, the primary influencing parameter is the spatial variation of the main fibre orientation, which governs the first-order anisotropic behaviour of the material. These results suggest that the use of such effective media is particularly relevant for the simulation of UT procedures. In particular, the proposed framework can be effectively employed for:

– the computation of delay laws and the correction of time-of-flight values used in Total Focusing Method (TFM) imaging,
– the estimation of beam deviations induced by material anisotropy,
– and the evaluation of attenuation losses associated with qL wave scattering.

The imperfect fit observed for shear wave attenuation can be attributed to the higher sensitivity of these modes to microstructural features such as orientation distributions and grain shape including strong elongation. These scattering effects are only partially captured by the effective medium approximation and it remains more challenging to predict accurately losses for qSV and qSH waves.

In practice, weld inspection is predominantly performed using longitudinal waves, particularly when the aim is to detect defects behind the weld. In this case, shear wave fronts are generally far too attenuated and distorted, and are therefore more difficult to observe experimentally. As a result, the larger modelling errors associated with shear wave attenuation have a limited impact on most practical UT applications.

5 Conclusion and perspectives

This study presents a comprehensive and robust workflow for characterising wave scattering in textured polycrystalline materials, using the single-crystal properties of cubic austenite as a baseline. By leveraging parametric statistics, the definition of microstructures is simplified, enabling a systematic analysis of their influence on wave propagation. The methodology relies on parametric fibre-Gaussian crystallographic ODFs, but can be readily extended to other parametric ODF formulations. Grain size D and elongation factor E distributions can also be incorporated, allowing the modelling of microstructures ranging from equiaxed to epitaxial.

The effective macroscale properties of these textured materials have been successfully estimated using an anisotropic viscoelastic model. This approach establishes a direct link between microstructural parameters and effective stiffness components governing coherent wave behaviour.

The proposed workflow is particularly well suited for UT simulations and imaging applications. In particular, it enables the estimation of representative stiffness tensors for UT simulations in welded components. By improving the understanding of anisotropy variability and attenuation effects, this approach supports more accurate parametric studies in UT process simulations, such as those performed using the CIVA software platform developed by CEA. Furthermore, it provides a consistent framework for correcting ToF matrices and adapting TFM imaging in complex welded structures [22, 23].

Overall, this approach enhances the predictive capability of wave propagation models and opens new perspectives for improving UT techniques in applications involving textured structures. Future work will focus on further automating the workflow in order to construct comprehensive metamodels, thereby facilitating the integration of effective material properties into our advanced UT simulation tools. We will also analyse how the effective properties vary with frequency according to diffusion regimes in such textured materials and examine the frequency-dependent relationships between the velocity and attenuation of the identified coherent modes.

Funding

The authors gratefully acknowledge the financial support provided by EDF for this study.

Conflicts of interest

The authors declare that they have no known competing financial interests or personal relationships that could have appeared to influence the work reported in this paper.

Data availability statement

Data are available on request from the authors.

Author contribution statement

Nicolas Leymarie: Conceptualization, Methodology, Formal analysis, Writing – Original draft. **Vincent Dorval:** Conceptualization, Methodology, Software, Writing – Review & Editing. **Jordan Barras:** Conceptualization, Methodology, Software, Writing – Review & Editing. **Alexandre Imperiale:** Software, Writing – Review & Editing. **Edouard Demaldent:** Supervision, Writing – Review & Editing.

References

1. F.E. Stanke, G.S. Kino: A unified theory for elastic wave propagation in polycrystalline materials. The Journal of the Acoustical Society of America 75, 3 (1984) 665–681.
2. R.L. Weaver: Diffusivity of ultrasound in polycrystals. Journal of the Mechanics and Physics of Solids 38, 1 (1990) 55–86.
3. M. Huang, S.I. Rokhlin, M.J.S. Lowe: Appraising scattering theories for polycrystals of any symmetry using finite elements. Philosophical Transactions of the Royal Society A: Mathematical, Physical and Engineering Sciences 380, 2231 (2022) 20210382.
4. L. Yang, O. Lobkis, S. Rokhlin: Shape effect of elongated grains on ultrasonic attenuation in polycrystalline materials. Ultrasonics 51, 6 (2011) 697–708.
5. M. Huang, G. Sha, P. Huthwaite, S.I. Rokhlin, M.J.S. Lowe: Longitudinal wave attenuation in polycrystals with elongated grains: 3D numerical and analytical modeling. The Journal of the Acoustical Society of America 149, 4 (2021) 2377–2394.
6. J.C. Victoria-Giraldo, B. Tie, J. Laurent, A. Lhémery, D. Solas: Ultrasonic scattering in polycrystalline materials with elongated grains: a comparative 3D and 2D theoretical and numerical analysis. Ultrasonics 152 (2025) 107642.
7. S. Ahmed, R.B. Thompson: Propagation of elastic waves in equiaxed stainless-steel polycrystals with aligned [001] axes. The Journal of the Acoustical Society of America 99, 4 (1996) 2086–2096.
8. J.A. Turner: Elastic wave propagation and scattering in heterogeneous, anisotropic media: textured polycrystalline materials. The Journal of the Acoustical Society of America 106, 2 (1999) 541–552.
9. J. Li, S. Rokhlin: Propagation and scattering of ultrasonic waves in polycrystals with arbitrary crystallite and macroscopic texture symmetries. Wave Motion 58 (2015) 145–164.
10. A. Van Pamel, C.R. Brett, P. Huthwaite, M.J.S. Lowe: Finite element modelling of elastic wave scattering within a polycrystalline material in two and three dimensions. The Journal of the Acoustical Society of America 138, 4 (2015) 2326–2336.
11. M. Ryzy, T. Grabec, P. Sedlák, I.A. Veres: Influence of grain morphology on ultrasonic wave attenuation in polycrystalline media with statistically equiaxed grains. The Journal of the Acoustical Society of America 143, 1 (2018) 219–229.
12. P.E. Lhuillier, B. Chassignole, M. Oudaa, S.O. Kerhervé, F. Rupin, T. Fouquet: Investigation of the ultrasonic attenuation in anisotropic weld materials with finite element modeling and grain-scale material description. Ultrasonics 78 (2017) 40–50.
13. V. Dorval, N. Leymarie, A. Imperiale, E. Demaldent, P.-E. Lhuillier: Numerical estimation of ultrasonic phase velocity and attenuation for longitudinal and shear waves in polycrystalline materials. Ultrasonics 148 (2025) 107517.
14. V. Dorval, N. Leymarie, A. Imperiale, E. Demaldent, P.-E. Lhuillier: Numerical characterization of quasi-longitudinal and quasi-shear waves in anisotropic polycrystalline microstructures with elongation and texture. Ultrasonics 161 (2026) 107935.
15. V. Dorval, N. Leymarie, A. Imperiale, E. Demaldent: Multi-modal characterization of ultrasonic bulk wave properties in heterogeneous textured media through finite element computations. Journal of Physics: Conference Series 2904, 1 (2024) 012005.
16. H.M. Ledbetter: Monocrystal elastic constants in the ultrasonic study of welds. Ultrasonics 23, 1 (1985) 9–13.
17. B.A. Auld: Acoustic Fields and Waves in Solids. Vol. 1. Krieger, 1990.
18. B. Castagnède, J.T. Jenkins, W. Sachse, S. Baste: Optimal determination of the elastic constants of composite materials from ultrasonic wave-speed measurements. Journal of Applied Physics 67, 6 (1990) 2753–2761.
19. C. Aristégui, S. Baste: Optimal recovery of the elasticity tensor of general anisotropic materials from ultrasonic velocity data. The Journal of the Acoustical Society of America 101, 2 (1997) 813–833.

20. B. Chassignole, V. Duwig, M.A. Ploix, P. Guy, R. El Guerjouma: Modelling the attenuation in the ATHENA finite elements code for the ultrasonic testing of austenitic stainless steel welds. Ultrasonics 49, 8 (2009) 653–658.
21. N. Leymarie, A. Imperiale, T. Fortuna, E. Demaldent: Comparisons of ray and finite element simulations of ultrasonic wave fields in smoothly inhomogeneous austenitic welds of thick-walled components. NDT & E International 147 (2024) 103177.
22. C. Ménard, S. Robert, R. Miorelli, D. Lesselier: Optimization algorithms for ultrasonic array imaging in homogeneous anisotropic steel components with unknown properties. NDT & E International 116 (2020) 102327.
23. M.K. Kalkowski, M.J.S. Lowe, V. Samaitis, F. Schreyer, S. Robert: Weld map tomography for determining local grain orientations from ultrasound. Proceedings of the Royal Society A: Mathematical, Physical and Engineering Sciences 479, 2277 (2023) 20230236.

Cite this article as: Leymarie N. Dorval V. Barras J. Imperiale A. & Demaldent E. 2026. Numerical characterisation of elastic wave propagation in fibre-textured polycrystals: Example of complex-valued stiffness evolution with microstructural parameters. Acta Acustica, **10**, 62. https://doi.org/10.1051/aacus/2026059.